Numerical simulation of wire-coating: the influence of temperature boundary conditions

Peter Wapperom
Ole Hassager

DPC (Danish Polymer Centre)
Institut for Kemiteknik
Danmarks Tekniske Universitet
DK-2800 Lyngby (Danmark)

Abstract

A finite element program has been used to analyze the wire-coating process of an MDPE melt. The melt is modelled by a nonisothermal Carreau model. The emphasis is on predicting an accurate temperature field. Therefore, it is necessary to include the heat conduction in the metal parts. A comparison is made with the results of a simulation that models the heat conduction in the metal head by means of a Biot boundary condition. The influence of the wire velocity, inlet temperature and power-law index will be examined.

Keywords: polymeric fluids; wire coating; Carreau model; nonisothermal; finite elements; temperature boundary conditions

1 Introduction

The coating of metal wires by extrusion is an important process for cable companies. Empirical optimization of the process is often difficult, expensive and time consuming. Therefore numerical simulations have become more popular. In recent years various papers have been presented on the numerical simulation of the wire-coating process. Caswell & Tanner [1] started with simulation of isothermal flow, using the finite element method. Later on non-isothermal effects have been taken into account by [2], [3], [4], [5] and [6]. A good prediction of the temperature is important, because the viscosity depends strongly on temperature and because too high temperatures may cause degradation or too early cross-linking of the polymer. Relatively little attention has been paid to thermal boundary conditions. In the die, the temperature is usually controlled at some distance from the metal head-polymer interface. This temperature is then assumed as boundary condition on that surface, see [2], [3] and [4]. However, due to the high viscous dissipation near the metal head, that boundary condition is rather unrealistic. Therefore, in a key development on the modelling of wire coating operations Mitsoulis *et al.* [5] have formulated a more realistic boundary condition. They showed that such a temperature boundary condition results in a considerable temperature rise at the metal head-polymer interface. That boundary condition is based on the 1D problem of steady heat conduction in radial direction through a metal head of fixed inner and outer radius, assuming no axial heat conduction and fixed temperatures at the inner and outer radius. The result is formulated in the form of a 1D Biot condition. While this represents a major improvement in the temperature boundary condition over the the fixed temperature condition, it is not a priori clear how good this one is. The metal head-polymer interface does not have a constant radius and the temperature along that interface is not constant. Consequently axial heat conduction in the metal head could be substantial. Furthermore, the boundary condition can not be applied at the inner radius of the polymer channel, because the temperature is not controlled in the interior and therefore the temperature at the inner radius of the 1D problem is not known.

In this article we will take into account the heat conduction in the metal parts as well, by including these in the domain of solution and solving extra finite element equations for the temperature in the metal head and wire. We will focus on the temperature and pressure drop and compare the results with the boundary conditions previously used.

2 Geometry

For the coating problem the standard geometry we will use, is sketched in Fig. 1 (not real scale). The coordinates of the various points are given in Table 1. The geometry consists of a polymer channel, a metal head and a copper wire [7].

The copper wire is pulled with a constant speed and coated with a thin layer of hot polymer at line IJ. At the free boundary the polymer melt is cooled by means of a water bath from point G till H. At the first part of the free boundary, from point F to G, the polymer is surrounded by air. Initially, the polymer melt is also cooled via the copper wire, because the copper wire usually has a much lower temperature.

3 Governing equations

3.1 Equations for the polymer melt

The mathematical model we have used to describe the nonisothermal flow of polymeric fluids is well-known, see for example [8] Sec. 1.2 and 4.1.

For steady and incompressible flow the balance of mass and the balance of linear momentum become

$$\nabla \cdot \boldsymbol{v} = 0, \tag{1}$$

$$\rho \boldsymbol{v} \cdot \nabla \boldsymbol{v} + \nabla p = \nabla \cdot \boldsymbol{\sigma}, \tag{2}$$

where $\boldsymbol{v}$ is the velocity, ρ the fluid density, p the pressure and $\boldsymbol{\sigma}$ the extra-stress tensor.

The extra-stress tensor $\boldsymbol{\sigma}$ has to be specified by a constitutive equation. For viscous fluids $\boldsymbol{\sigma}$ is related to the Euler rate-of-deformation tensor $\boldsymbol{d}$ by

$$\boldsymbol{\sigma} = 2\eta \boldsymbol{d}, \tag{3}$$

where η is the viscosity and $\boldsymbol{d} = (\nabla \boldsymbol{v} + (\nabla \boldsymbol{v})^T)/2$. For the dependence of the viscosity on shear rate, we will use the Carreau model:

$$\eta = \eta_0 \left(1 + 2\lambda^2 |\boldsymbol{d} : \boldsymbol{d}|\right)^{\frac{n-1}{2}}, \tag{4}$$

where η_0 is the zero-shear-rate viscosity, n the power-law index and λ a time constant that determines the length of the viscosity plateau for low shear rates. The viscosity η_0 and the time constant λ depend strongly on temperature. We describe the temperature dependence by an Arrhenius shift factor a_T:

$$\log_{10}\left(\frac{\lambda}{\lambda_{\text{ref}}}\right) = \log_{10}\left(\frac{\eta_0}{\eta_{0,\text{ref}}}\right) = \log_{10} a_T = C\left(\frac{1}{T} - \frac{1}{T_{\text{ref}}}\right), \tag{5}$$

where the subscript $_{\text{ref}}$ denotes a quantity at reference temperature T_{ref}, the absolute temperature is denoted T and C a constant.

For steady incompressible flow of a viscous fluid the temperature equation becomes

$$\rho c_p \boldsymbol{v} \cdot \nabla T = 2\eta \boldsymbol{d} : \boldsymbol{d} + \nabla \cdot (\kappa \nabla T), \tag{6}$$

where c_p is the heat capacity at constant pressure and κ the thermal conductivity.

3.2 Equations for the metal parts

The copper wire is pulled with a constant speed V_{w}. However, the temperature of the copper wire is not known a priori. Although the thermal conductivity of the copper wire is much larger than that for the polymeric fluid, it is not expected that a constant temperature boundary condition is very accurate. Due to the large temperature difference between the polymer and the wire, and the small diameter of the wire the temperature will certainly change. Therefore, we solve an extra temperature equation for the copper wire

$$\rho_{\text{c}} c_{p,\text{c}} V_{\text{w}} \frac{\partial T}{\partial z} = \nabla \cdot (\kappa_{\text{c}} \nabla T), \tag{7}$$

where ρ_{c} is the density, $c_{p,\text{c}}$ the heat capacity and κ_{c} the thermal conductivity of the copper wire. For the calculations we will assume constant physical properties.

In the given equipment the temperature is controlled at the outer boundary of the metal head. Due to mechanical dissipation in the polymer flow, the temperature near the metal head-polymer interfaces, the lines AF and LQ in Fig. 1, will rise. To take into account the resulting heat conduction in the metal head, we will also solve the temperature equation in the metal head:

$$\nabla \cdot (\kappa_{\text{h}} \nabla T) = 0, \tag{8}$$

where κ_{h} is the thermal conductivity of the metal head. We will assume a constant κ_{h}.

3.3 Numerical method

To solve the system of equations we have used the finite element package SEPRAN [9]. We have used standard numerical methods, so we will describe them very briefly. For the equations of motion the Crouzeix–Raviart element has been used, in combination with the penalty method to fulfil the balance of mass (1), see [10] p. 263. The free boundary is computed with the help of the film method described in [11]. For the temperature the standard quadratic element has been used. To handle the high Péclet numbers SUPG upwinding has been used, as described in [12]. The resulting discretized system of equations has been solved by an iterative method, using a simple successive substitution scheme.

4 Material properties

4.1 Properties of medium density polyethylene ME 4425

The polymer used for coating is the medium density polyethylene (MDPE) melt ME 4425. For the viscosity of ME 4425 for the small-amplitude oscillatory shear flow, data have been made available by NKT Cables A/S. The magnitude of the complex viscosity $|\eta^*|$ is known as function of frequency in the range $6 \cdot 10^{-2}$ s^{-1} $< \omega <$ $2 \cdot 10^2$ s^{-1}, at three different temperatures: $T = 433$ K, $T = 463$ K and $T = 493$ K. To find the viscosity as function of the shear rate, the Cox–Merz rule has been applied (see for example [8]):

$$\eta(\dot{\gamma}) = |\eta^*(\omega)|_{\omega=\dot{\gamma}} \,. \tag{9}$$

Fig. 2 shows the data points and the curves of the Carreau model with an Arrhenius shift factor. The parameters used for the model are given in Table 2. The correspondence between the Carreau model and the experimental data is good in the power-law region. For low shear rates (frequencies) the viscosity is overpredicted by the Carreau model. Probably, this is not very important because the shear rates are very high in coating flows. Unfortunately, no data could be made available for $\omega > 2 \cdot 10^2$ s^{-1} which is more severe drawback. The more so as we will show in Sec. 6 that a good fit of the viscosity at high shear rates is very important for the resulting pressure drop and maximum temperature, and that for the coating flow very high shear rates of $\mathcal{O}$ (10^4 s^{-1}) are not unusual. The temperature dependence of the MDPE melt is similar to LDPE, for which the same shift constants apply [8] p. 140.

Other properties that were available for ME 4425 are given in Table 2 as well. For the thermal properties that could not be made available, we have taken the values of LDPE. For the temperature dependence of the heat capacity we have used the linear relation

$$c_p(T) = c_p(T_{\text{ref}}) \left(1 + \alpha_c (T - T_{\text{ref}})\right) , \tag{10}$$

with the values for LDPE $c_p(T_{\text{ref}}) = 2.57 \cdot 10^3$ J $\cdot$ kg^{-1} $\cdot$ K^{-1} and $\alpha_c = 1.0 \cdot 10^{-3}$ K^{-1}, see [8] Table 4.4-2 and [13] Table 9.7.

The thermal conductivity is only known at $T = 297.5$ K. For polyethylene melts the thermal conductivity usually decreases with increasing temperature until a certain lower bound. Therefore, we have used the linear relation

$$\kappa(T) \quad = \quad \kappa(T_{\text{ref}}) \left(1 + \alpha_\kappa (T - T_{\text{ref}})\right) , \tag{11}$$

for $T < 400$ K and a constant thermal conductivity of $\kappa = 0.26$ W $\cdot$ m^{-1} $\cdot$ K^{-1} above this temperature. For the thermal conductivity at the reference temperature $T_{\text{ref}} = 297.5$ K the

measured value of Table 2 has been used. For the temperature dependence of the thermal conductivity this gives $\alpha_\kappa = -2.0 \cdot 10^{-3}$ K^{-1}.

The flow rate at the inflow can be calculated with the help of an overall mass balance. To obtain a coating layer of thickness $R_\mathrm{c} = R_\mathrm{H} - R_\mathrm{I}$ we need a flow rate at the inlet of

$$Q_\mathrm{i} = \pi V_\mathrm{i}(R_\mathrm{A}^2 - R_\mathrm{Q}^2) = \frac{\rho_\mathrm{o}}{\rho_\mathrm{i}} \pi V_\mathrm{o}(R_\mathrm{H}^2 - R_\mathrm{I}^2), \tag{12}$$

where the R-subscripts refer to the points in Fig. 1 and $_\mathrm{i}$ and $_\mathrm{o}$ denote the inlet and outlet. The velocity V_o equals V_w, the velocity of the wire. The difference in density at inlet conditions of $p = \mathcal{O}(10^7)$ Pa and $T = 463$ K and outlet conditions of $p = 10^5$ Pa and $T = 293$ K is about $\rho_\mathrm{o}/\rho_\mathrm{i} = 1.14$ for LDPE. We will also use this value for the MDPE melt and adjust Q_i to obtain $R_\mathrm{c} = 0.7$ mm according to Eq. 12. Because we assume incompressible flow, this means that the thickness of the coating layer resulting from the computations is somewhat larger than $R_\mathrm{c} = 0.7$ mm. On the other hand, we obtain more accurate (higher) velocities in the die than we would obtain with the flow rate based on the outlet conditions and a ratio of $\rho_\mathrm{o}/\rho_\mathrm{i} = 1$.

4.2 Other material properties

For the numerical simulation of the coating flow, the material properties of the surrounding metal parts and fluids are needed as well. We have obtained those properties from [14].

The properties of the metal parts are given in Table 3. Because these properties are not very sensitive to temperature changes, we will take them constant in the numerical simulations. The head is iron based. For the thermal conductivity we will take the value of iron at 500 K. For the copper wire we will take the properties at $T = 400$ K.

For the boundary conditions at the free surface, see Sec. 5, we need the properties of water and air. The necessary properties at $T = 373$ K and $p = 10^5$ Pa, are summarized in Table 4 for water and in Table 5 for air.

5 Boundary conditions

At the boundaries of the geometry sketched in Fig. 1, boundary conditions have to be specified for the equations of motion and the temperature equation. Next, we will discuss these boundary conditions with the emphasis on the temperature boundary conditions.

- **at the inlet of the polymer**: Fully developed velocity profile with given flow rate Q_i, and fixed temperature $T = T_\mathrm{p}$. Unless explicitly stated, we will take $T_\mathrm{p} = 463$ K.

- **at the inlet of the copper wire**: Fixed temperature $T = T_c$. In our computations we will take $T_c = 383$ K.

- **at the metal head-polymer interface**: Vanishing velocity $\boldsymbol{v} = \boldsymbol{0}$ and continuous temperature and normal component of the heat flux. For comparison we will also consider the case where the heat conduction in the metal head is not included explicitly, but modelled by the Biot boundary condition $\kappa \boldsymbol{n} \cdot \nabla T = -h(T - T_0)$ as used in [5]. The parameter h is determined with the help of the analytical solution of the steady 1D heat conduction problem in a metal tube with constant temperatures at the inner radius R_1 and outer radius R_2. For our coating problem T_0 is the controlled temperature (equal to the inlet temperature T_p) at the outer radius of the metal head R_2 and

$$h = \frac{\kappa_m}{R_1} \frac{1}{\ln R_1/R_2}. \tag{13}$$

  Because the inner radius of the outer part of the metal head is not constant it is not clear what has to be taken for R_1. For our calculations we will take $R_1 = 1.8$ mm, which corresponds to the radius at point F, and $R_1 = 13.4$ mm which corresponds to the averaged radii of point A and F. This results in $h = 9.9 \cdot 10^3$ W $\cdot$ m$^{-2} \cdot$ K and $h = 3.2 \cdot 10^3$ W $\cdot$ m$^{-2} \cdot$ K respectively. The value $R_1 = 1.8$ mm is chosen to obtain a good boundary condition near the zone with the highest dissipation, at the metal head before point F. At the inner boundary it is much more difficult to apply the Biot boundary condition, because the temperature is not controlled at the inner part of the metal head. Therefore, we will take as boundary condition $T = T_p$ with T_p the temperature of the polymer at the inlet, just as in [5].

- **at the free surface**: For the coating geometry of NKT Cables A/S, the first 0.35 m the polymer is surrounded by air. Then the polymer is cooled in water for about 30-40 m.

  The boundary conditions for the equations of motion are a vanishing normal velocity $\boldsymbol{v} \cdot \boldsymbol{n} = 0$ and a vanishing normal and tangential stress. For the temperature boundary condition we will take a Biot condition of the form

$$\kappa \boldsymbol{n} \cdot \nabla T = -h_m(T - T_0), \tag{14}$$

  where T_0 is the temperature of the surroundings and h_m a heat-transfer coefficient. The transfer of heat from the polymer wire will be modelled by free convection from a long horizontal cylinder. Except for a very small distance near point F, the diameter is constant (if density effects are neglected) and the coated wire is approximately a

long horizontal cylinder. The heat-transfer coefficient is given in terms of the non-dimensional Nusselt number:

$$Nu_m = \frac{h_m D}{\kappa_f}, \tag{15}$$

where h_m is the heat-transfer coefficient for the total surface of the cylinder, D the diameter of the cylinder and κ_f the thermal conductivity in the film around the cylinder. A subscript $_f$ denotes that a quantity has to be evaluated at the film temperature, for which usually the average of the polymer temperature and the temperature of the surroundings is taken: $T_f = (T_\mathrm{p} + T_0)/2$.

The Nusselt number for free convection from long horizontal cylinders equals (see [15] p. 413):

$$Nu_m = 0.518 \cdot (GrPr)^{0.25}, \tag{16}$$

for $GrPr > 10^4$, where the Prandtl number Pr and the Grashof number Gr are defined by

$$Pr = \frac{c_{p,f}\eta_f}{\kappa_f}, \tag{17}$$

$$Gr = \frac{D^3 \rho_f^2 g \beta_f \Delta T}{\eta_f^2}, \tag{18}$$

where g is the acceleration due to gravity and ΔT a characteristic temperature difference, the difference between the temperature of the polymer and the surroundings $\Delta T = T_\mathrm{p} - T_0$. If we take $T_\mathrm{p} = 463$ K and $T_0 = 293$ K we obtain for the film temperature $T_\mathrm{f} = 378$ K, which is just in the vapor phase at atmospheric pressure. So, it seems likely that the water is boiling at the first part of the water cooling. Cooling by a boiling fluid is a much more complicated problem [15]. Therefore, we will assume a non-boiling fluid with film temperature $T_\mathrm{f} = 373$ K for the properties of water. The thermal expansion coefficient that we use is based on the densities at 372.9 and 373 K.

Using the properties of water of Table 4 and $D = 2.8 \cdot 10^{-3}$ m and $\Delta T = 170$ K, gives $Pr = 1.6$ and $Gr = 3.5 \cdot 10^5$. From (15) and (16) we obtain for the heat-transfer coefficient $h_m = 3.4 \cdot 10^3$ W $\cdot$ m$^{-2} \cdot$ K. For air we find with the help of Table 5 that $Pr = 0.69$ and $Gr = 1.7 \cdot 10^2$, so that $GrPr < 10^4$. For the heat-transfer coefficient we obtain $h_m = 27$ W $\cdot$ m$^{-2} \cdot$ K, see [15] p. 413.

- **at the outer part of the metal head**: In the metal head the temperature is controlled at the outer boundary, corresponding to the line XY in Fig. 1, where we will assume a fixed temperature $T = T_\mathrm{h}$. Unless explicitly stated, we will take $T_\mathrm{h} = 463$ K. This

temperature will also be assumed (by lack of a better, measured, boundary condition) at the line AX, which is in the interior of the metal head. However, it is not likely that small variations of the temperature on this boundary have a large influence on the polymer temperature. At the line FY where the metal head is in contact with the air, we will assume a similar natural boundary condition as for the polymer-air interface. For a thin vertical plate the Nusselt number equals

$$Nu_m = 0.59 \cdot (GrPr)^{0.25}, \tag{19}$$

for $10^4 < PrGr < 10^9$, see [15] p. 414. The characteristic length D is the height of the plate. Although our plate is not thin, we will use this formula by lack of a better one. For air we find with $D = 5.32 \cdot 10^{-2}$ m: $Pr = 0.69$ and $Gr = 1.1 \cdot 10^6$. This gives a heat-transfer coefficient of $h_m = 11\ \mathrm{W \cdot m^{-2} \cdot K^{-1}}$.

- **at the inner part of the metal head**: At the line RQ which is in the interior of the metal head we will assume (by lack of a better, measured, boundary condition) $T = T_\mathrm{h}$, just as for the boundary AX of the outer part of the metal head. It is also difficult to find a good boundary condition on the contact line with the air, because the surrounding air is in a small closed chamber. We will assume a Biot boundary condition for the temperature $\kappa_\mathrm{h} \boldsymbol{n} \cdot \nabla T = -h(T - T_1)$. It is likely that the temperature in the chamber is determined by the temperature of the metal head, because its extent is much larger than that of the copper wire. Therefore, we will take $T_1 = T_\mathrm{h}$ with T_h the controlled temperature in the outer part of the head. For the heat transfer coefficient we will take $h = 1\ \mathrm{W \cdot m^{-2} \cdot K^{-1}}$. It is not clear what the influence of this boundary condition is or whether it is very important.

- **at the boundary JK**: In the real geometry this is a small free boundary. However, to avoid complications with the free boundary, we will assume a fixed wall, i.e. $\boldsymbol{v} = \boldsymbol{0}$. This means that we introduce a jump in the velocity at the point J, where the axial velocity equals V_m. Locally, this may lead to an unrealistic solution (large negative pressures), see also [1]. However, this is only restricted to a small region next to the point J. As temperature boundary condition we will take the same boundary condition as for the contact line of the metal wire and the the metal head with the surrounding air in the chamber: $\kappa \boldsymbol{n} \cdot \nabla T = -h(T - T_\mathrm{h})$ with $h = 1\ \mathrm{W \cdot m^{-2} \cdot K^{-1}}$ and T_h the controlled temperature.

- **at the copper wire-polymer interface**: continuous temperature and normal component of the heat flux, and no-slip boundary condition for the velocity, i.e. a constant tangential velocity $\boldsymbol{v} \cdot \boldsymbol{t} = V_{\mathrm{w}}$ and a vanishing normal velocity $\boldsymbol{v} \cdot \boldsymbol{n} = 0$ at line IJ.

- **at the axis of symmetry of the copper wire**: vanishing normal heat flux $\kappa_{\mathrm{c}} \boldsymbol{n} \cdot \nabla T = 0$ at line VW.

- **at the surface of the copper wire within the die**: As for line RK of the inner part of the metal head, it is difficult to find a good temperature boundary condition on the line UJ. We will assume a similar boundary condition as for the inner boundary of the metal head: $\kappa_{\mathrm{c}} \boldsymbol{n} \cdot \nabla T = -h(T - T_{\mathrm{h}})$ with $h = 1\ \mathrm{W} \cdot \mathrm{m}^{-2} \cdot \mathrm{K}^{-1}$ and T_{h} the controlled temperature. Due to the high speed and the low residence time of the wire in the chamber, the choice of h is probably not very important.

- **at the outlet of the polymer**: vanishing normal stress, vanishing tangential velocity $\boldsymbol{v} \cdot \boldsymbol{t} = 0$, and vanishing normal heat flux $\kappa \boldsymbol{n} \cdot \nabla T = 0$, at line HI.

- **at the outlet of the copper wire**: vanishing normal heat flux $\kappa_{\mathrm{c}} \boldsymbol{n} \cdot \nabla T = 0$ at line IW.

6 Results

In this section we present the results of a simulation including the heat conduction in the metal head. We will compare the results with the case the heat conduction in the metal head is modelled by a boundary condition. Furthermore, we will discuss the effect of the power-law index n, the temperature of the polymer at the inlet and the wire velocity.

6.1 Influence of the temperature boundary condition

To investigate the influence of the heat conduction in the metal head on the temperature near the wall, we have compared the results of a simulation including the metal head with numerical simulations without the metal head. For the latter case we have used the boundary condition (13) at the outer radius of the polymer channel.

Fig. 3 shows the radial temperature distributions in the polymer channel at various z-coordinates for the case that the metal head is taken into account. Results are displayed as function of the local radial coordinate in the channel: $r^*(r, z) = [r - R_{\mathrm{i}}(z)]/[R_{\mathrm{o}}(z) - R_{\mathrm{i}}(z)]$, where R_{i} and R_{o} denote the inner and outer radius of the polymer channel, respectively. A severe temperature rise occurs due to mechanical dissipation near the die walls. At the inner wall this effect is much larger than at the outer wall of the polymer channel, because

the temperature is controlled at the outer radius of the metal head. The latter results in a cooling effect at the outer wall of the polymer channel. The temperature rise is restricted to a thin boundary layer near the channel walls. In the centre of the polymer channel the temperature remains unchanged due to the dominance of convection, as can be observed more easily from Fig. 4, which displays temperature isolines in the die and polymer channel. This allows one to discern the heat transport, perpendicular to the isolines, in the polymer and the metal head. Fig. 5 reflects the isolines near the die exit in more detail. Particularly near the inner wall the temperature gradients are very steep. Also note that the isolines in the polymer intersect the die wall under a small angle and bend away almost perpendicularly in the metal head. This is caused by the fact that the thermal conductivity of the metal head is much larger than that of the polymer.

Fig. 6 shows the radial temperature distributions at various z-coordinates outside the head. First, the polymer is strongly cooled at the free boundary and at the copper wire ($z = 1000$ mm). For larger values of z the maximum temperature of the polymer fluid is at the copper wire-polymer interface and for large values of z the temperature profile is almost linear.

Figs. 7 and 8 show the radial temperature distributions at the same z-coordinates with the heat flux boundary condition (13) at the wall with $R_1 = 1.8$ mm and $R_1 = 13.4$ mm respectively. For the case with $R_1 = 13.4$ mm the temperatures at the outer wall are too high near the end of the die ($z = -5$ mm and $z = 0$). However, the maximum temperatures at a small distance from the outer wall are hardly influenced. For the no-flow zone near point D the temperature is too low. This is caused by the too strong cooling on the line DE: although this line is almost perpendicular to the direction of the heat conduction (about the r-direction) the same boundary condition is applied. The similar effect can be observed for the case with $R_1 = 1.8$ mm. For this case the temperature profile near the outer wall for $z = 0$ corresponds better to Fig. 3. For other z-values, however, the temperature profiles obtained with $R_1 = 13.4$ mm are better. The temperature profiles outside the head resemble closely to the ones in Fig. 6 and are therefore not shown.

Results for the maximum temperature and the position of it and the total pressure drop are given in Table 6. For comparison the results for an adiabatic boundary condition at the outer wall of the polymer channel are given as well. Note that the maximum temperature for the simulation that do not include the metal head is at or near point F, while for the simulation including the metal head it is at the inner wall. For the latter the temperature

at point F is about 490 K as can be seen in Fig. 6. The pressure drop is large at the end of the converging section, near point L. Nevertheless, the influence of the different temperature profiles at that place on the pressure drop is relatively small, even for the adiabatic case, because the temperature rise is only large in a narrow region near the wall close to points L and F. The temperatures at the exit are not influenced by the presence of a metal head in the computations. For all four cases the temperature at the wire-polymer interface is $T_{\mathrm{wire,ex}} = 346$ K and at the water-polymer interface $T_{\mathrm{water,ex}} = 298$ K. We conclude from Table 6, that a careful simulation of the conduction in the metal head is essential for the estimation of the maximum temperature in the process.

6.2 Influence of the power-law index

We have investigated three different power-law indices: $n = 0.4$, $n = 0.47$ and $n = 0.55$. The viscosity functions are given in Fig. 9.

Results for the maximum temperature (just before point L at $z = -0.29$ mm, $r = 1.57$ mm), the temperatures at the metal wire-polymer interface and the polymer-air interface at the exit, and the total pressure drop are given in Table 7. The influence on the temperatures at the exit is small. However, both the maximum temperature and the pressure drop are very sensitive to the power-law index. Due to the higher viscosity for higher n the dissipation, and thus the temperature near the wall, and the pressure drop may increase considerably. Thus a good fit of the viscosity at high shear rates is indispensable for a correct prediction of the pressure drop and maximum temperature.

6.3 Influence of the inlet temperature

To investigate the influence of the inlet temperature at the polymer channel we have used three different temperatures $T_{\mathrm{p}} = 463$ K, $T_{\mathrm{p}} = 483$ K and $T_{\mathrm{p}} = 503$ K. The temperature of the head T_{h} has been adjusted similarly.

Results for the maximum temperature (just before point L at $z = -0.29$ mm, $r = 1.57$ mm), the temperatures at the metal wire-polymer interface and the polymer-air interface at the exit, and the pressure drop are given in Table 8. Due to a higher inlet temperature, the maximum temperature of course increases. However, less than the difference in the inlet temperature, because of the lower viscosity at higher temperatures (and thus a lower viscous dissipation). Due to the lower viscosity at higher temperatures, the pressure drop decreases with increasing inlet temperature. The influence of the temperature on the pressure drop is larger than for the temperature boundary conditions discussed in Sec. 6.1, because there

only the temperature close to the walls was affected. Thus a good approximation of the inlet temperature seems to be important, both for the pressure drop and the maximum temperature.

6.4 Influence of the wire velocity

To investigate the influence of the wire velocity, we have have taken $V_w = 10\ m \cdot s^{-1}$, $V_w = 20\ m \cdot s^{-1}$ and $V_w = 50\ m \cdot s^{-1}$. Simultaneously, we adjusted the flow rate, so that the thickness of the coating layer remained equal.

Results for the maximum temperature (just before point L at $z = -0.29$ mm, $r = 1.57$ mm), and the position of it, the temperatures at the metal wire-polymer interface and the polymer-air interface at the exit, and the total pressure drop are given in Table 9. The higher speeds give a much larger viscous dissipation near the walls, which results in very high maximum temperatures near point L. The increasing temperatures at the exit are caused by the higher Péclet numbers (higher wire velocity) outside the die. Furthermore, a higher wire velocity results in much higher pressure drops, although the viscosity strongly decreases due to shear thinning and the higher temperatures.

7 Conclusions

The wire-coating process of the polyethylene melt ME4425 has been analyzed numerically. For the prediction of the temperature rise due to dissipation, the temperature boundary conditions are very important, particularly at the walls. Due to the strong viscous dissipation near the walls and the dominance of convection in the centre of the polymer channel, the polymeric fluid is only heated near the walls. A large part of the fluid still has about the same temperature at the end of the die as at the inlet, so that the inlet temperature is important as well. Near the outer radius of the polymer channel a reasonable agreement with the temperature of simulations including the heat conduction in the metal head can be obtained with the help of a Biot boundary condition, at least if the outer boundary of the polymer channel does not contain sections that are about parallel to the radial direction. For the inner wall such a boundary is not possible, because the temperature is not controlled at the inner radius of the metal head. The temperature at the inner wall can be much larger than at the outer wall, so that it is important to take into account the heat conduction in the inner part of the metal head for a good prediction of the maximum temperature.

Although the various boundary conditions influence the (maximum) temperature considerably, the influence on the pressure drop is rather small. To obtain accurate predictions of

the pressure drop, and of course also for the maximum temperature, a good fit of the viscosity and the inlet temperature are very important. Increasing the production speed seems to be limited by the maximum temperature in the polymeric fluid. At high wire speeds viscous dissipation results in a very large temperature near the inner wall, well above the temperatures at which the polymer starts to cross-link and degrade.

8 Acknowledgements

The authors would like to thank Keld Venø Poulsen of NKT Cables A/S for making the wire-coating geometry available to us. Peter Wapperom was supported by the Danish Materials Technology Development Programme (MUP2) and the European Economic Community under the Human Capital programme (contract CHRX-CT93-0200).

References

[1] B. Caswell and R.I. Tanner, Polym. Eng. Sci. **18**, 416 (1978).

[2] R. Wagner and E. Mitsoulis, Adv. Polym. Technol. **5**, 305 (1985).

[3] J.F.T. Pittman and K. Rashid, Plast. Rub. Proc. Appl. **6**, 153 (1986).

[4] E. Mitsoulis, Pol. Eng. Sci. **26**, 171 (1986).

[5] E. Mitsoulis, R. Wagner and F.L. Heng, Pol. Eng. Sci. **28**, 291 (1988).

[6] P.G. Lafleur, B. Arpin and V. Lenir, Adv. Pol. Tech. **13**, 297 (1994).

[7] N. Lund and B. Høyer-Hansen, Isolering af elektriske ledere med PEX, Internal report of NKT (1995).

[8] R.B. Bird, R.C. Armstrong and O. Hassager, Dynamics of polymeric liquids, vol. 1, Fluid mechanics, John Wiley & Sons, New York (1987).

[9] A. Segal, Sepran manuals, Leidschendam (1984).

[10] C. Cuvelier, A. Segal and A.A. van Steenhoven, Finite Element Methods and Navier–Stokes Equations, D. Reidel Publishing Co., Dordrecht (1986).

[11] B. Caswell and M. Viriyayuthakorn, J. Non-Newtonian Fluid Mech. **12**, 13 (1983).

[12] A. Brooks and T.J.R. Hughes, Comp. Meth. Appl. Mech. Eng. **32**, 199 (1982).

[13] R.I. Tanner, Engineering rheology, Clarendon Press, Oxford (1985).

[14] R.H. Perry and D. Green, Perry's chemical engineering handbook (6th ed), McGraw Hill, New York (1984).

[15] R.B. Bird, W.E. Stewart and E.N. Lightfoot, Transport phenomena, John Wiley & Sons, New York (1960).

Table 1: Radial and axial coordinates (r, z) in mm of points A-Y in Fig. 1.

point	r	z
A	25.00	-61.0
B	25.00	-45.0
C	17.75	-31.0
D	17.75	-29.0
E	16.75	-29.0
F	1.80	5.0
G	-	35.0
H	-	$4.00 \cdot 10^4$
I	0.70	$4.00 \cdot 10^4$
J	0.70	0.0
K	1.00	0.0
L	1.45	0.0
M	15.37	-35.5

point	r	z
N	15.37	-33.0
O	16.37	-33.0
P	23.00	-45.0
Q	23.00	-61.0
R	8.00	-61.0
S	8.00	-35.0
T	1.00	-10.0
U	0.70	-61.0
V	0	-61.0
W	0	4.00
X	55.00	-61.0
Y	55.00	5.0

Table 2: Properties of ME 4425. Density at $T = 423$ K, thermal conductivity at $T = 297.5$ K, and viscosity constants used to fit shear viscosity in Fig. 2 with Carreau model and Arrhenius shift factor.

ρ	$7.85 \cdot 10^{2}$	$\mathrm{kg \cdot m^{-3}}$
κ	$3.3 \cdot 10^{-1}$	$\mathrm{W \cdot m^{-1} \cdot K^{-1}}$
η_0	$5.014 \cdot 10^{4}$	$\mathrm{Pa \cdot s}$
n	0.47	$-$
λ	$1.25 \cdot 10^{1}$	s
T_{ref}	$4.23 \cdot 10^{2}$	K
C	$1.95 \cdot 10^{3}$	K

Table 3: Properties of iron (metal head) at 500 K and copper (wire) at 400 K. Data from [14], p. 3-96, 3-130 and 3-261.

κ_{h}	$0.61 \cdot 10^2$	$\mathrm{W \cdot m^{-1} \cdot K^{-1}}$
ρ_{c}	$8.89 \cdot 10^3$	$\mathrm{kg \cdot m^{-3}}$
$c_{p,\mathrm{c}}$	$3.97 \cdot 10^2$	$\mathrm{J \cdot kg^{-1} \cdot K^{-1}}$
κ_{c}	$3.92 \cdot 10^2$	$\mathrm{W \cdot m^{-1} \cdot K^{-1}}$

Table 4: Properties of water at $T = 373$ K and $p = 10^5$ Pa. Data from [14], p. 3-70, 3-243 and 3-252.

ρ_w	$9.58 \cdot 10^2$	$\mathrm{kg \cdot m^{-3}}$
β_w	$6.89 \cdot 10^{-4}$	$\mathrm{K^{-1}}$
$c_{p,\mathrm{w}}$	$4.22 \cdot 10^3$	$\mathrm{J \cdot kg^{-1} \cdot K^{-1}}$
κ_w	0.68	$\mathrm{W \cdot m^{-1} \cdot K^{-1}}$
η_w	$0.26 \cdot 10^{-3}$	$\mathrm{Pa \cdot s}$

Table 5: Properties of air at $T = 378$ K and $p = 10^5$ Pa. Data from [14], p. 3-163 and 3-250.

ρ_a	$9.4 \cdot 10^{-1}$	$\mathrm{kg \cdot m^{-3}}$
β_a	$2.5 \cdot 10^{-3}$	$\mathrm{K^{-1}}$
$c_{p,\mathrm{a}}$	$1.01 \cdot 10^{3}$	$\mathrm{J \cdot kg^{-1} \cdot K^{-1}}$
κ_a	$3.2 \cdot 10^{-2}$	$\mathrm{W \cdot m^{-1} \cdot K^{-1}}$
η_a	$2.2 \cdot 10^{-5}$	$\mathrm{Pa \cdot s}$

Table 6: Maximum temperature and coordinates, temperature at wire-polymer interface at exit, temperature at water-polymer interface at exit, and pressure drop for various temperature boundary conditions.

Thermal boundary condition	z(mm)	r(mm)	$T_{\max}$(K)	$\Delta p(10^5$ Pa)
Conduction in metal head included	-0.29	1.57	504	117.5
Adiabatic boundary condition	4.79	1.89	523	114.6
Biot boundary condition ($R_1 = 1.8$ mm)	5.00	1.80	490	120.3
Biot boundary condition ($R_1 = 13.4$ mm)	5.00	1.80	496	119.3

Table 7: Maximum temperature and coordinates, temperature at wire-polymer interface at exit, and temperature at water-polymer interface at exit for various power-law indices.

n	$T_{\max}$(K)	$T_{\text{wire,ex}}$(K)	$T_{\text{water,ex}}$(K)	$\Delta p(10^5$ Pa)
0.40	487	345	298	69.6
0.47	504	346	298	117.5
0.55	536	348	298	207.0

Table 8: Maximum temperature and coordinates, temperature at wire-polymer interface at exit, temperature at water-polymer interface at exit, and total pressure drop for various temperatures at inlet.

T_{inlet}(K)	$T_{\max}$(K)	$T_{\text{wire,ex}}$(K)	$T_{\text{water,ex}}$(K)	$\Delta p(10^5$ Pa)
463	504	346	298	117.5
483	518	351	299	98.9
503	532	355	299	84.1

Table 9: Maximum temperature, temperature at wire-polymer interface at exit, temperature at water-polymer interface at exit, and total pressure drop for various wire velocities.

V_{w} $(\mathrm{m}\cdot\mathrm{s}^{-1})$	$T_{\max}$(K)	$T_{\mathrm{wire,ex}}$(K)	$T_{\mathrm{water,ex}}$(K)	$\Delta p(10^5$ Pa)
10	504	346	298	117.5
20	537	384	303	155.6
50	618	445	312	222.2

Figure 1: Sketch of flow geometry for coating of a metal wire.

Figure 2: Shear viscosity as function of shear rate for various temperatures, and Carreau model with parameters from Table 2. $\diamond$: 433 K, $+$: 463 K, $\square$: 493 K, dotted line: Carreau model at 433 K, $\cdot-$ line: Carreau model at 463 K, $\cdot\ -$ line: Carreau model at 493 K.

Figure 3: Temperature distribution in polymer channel at various z-coordinates as function of the local radial coordinate r^*; heat conduction in metal head taken into account.

Figure 4: Temperature distribution in the die; $0.7 < r < 28$ mm, $-61 < z < 5$ mm, eight contour lines distributed linearly between $T = 462$ and 404 K.

Figure 5: Temperature distribution near the die exit; $0.7 < r < 5$ mm, $-3 < z < 5$ mm, eight contour lines distributed linearly between $T = 462$ and 404 K.

Figure 6: Temperature distribution outside polymer channel at various z-coordinates as function of the local radial coordinate r^*; heat conduction in metal head taken into account.

Figure 7: Temperature distribution in polymer channel at various z-coordinates as function of the local radial coordinate r^*; heat conduction in metal head modelled by Eq. (13) with $R_1 = 1.8$ mm.

Figure 8: Temperature distribution in polymer channel at various z-coordinates as function of the local radial coordinate r^*; heat conduction in metal head modelled by Eq. (13) with $R_1 = 13.4$ mm.

Figure 9: Viscosity functions for various values of power-law index n in Carreau model. $n = 0.4$: dashed line with small dashes, $n = 0.47$: dashed line with large dashes, $n = 0.55$: solid line.

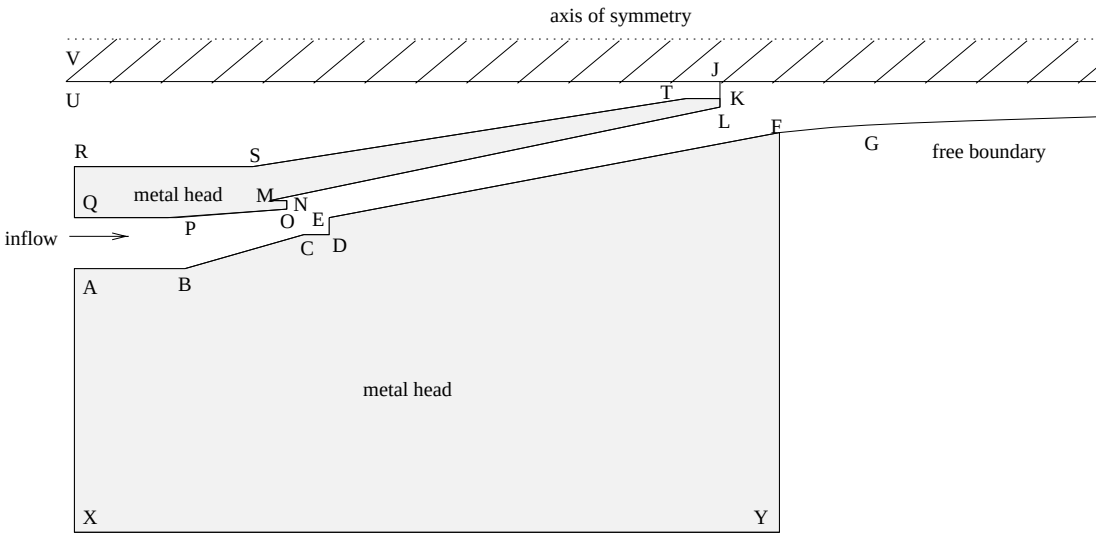

Wapperom, Fig. 1

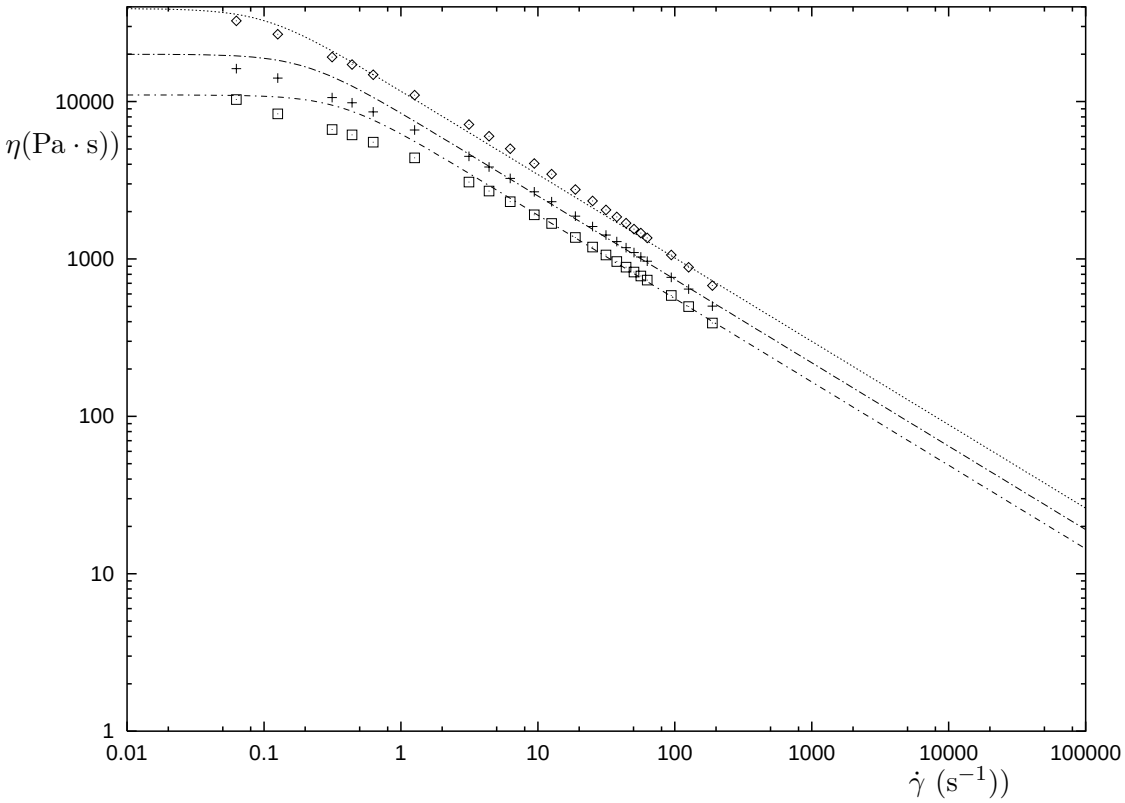

Wapperom, Fig. 2

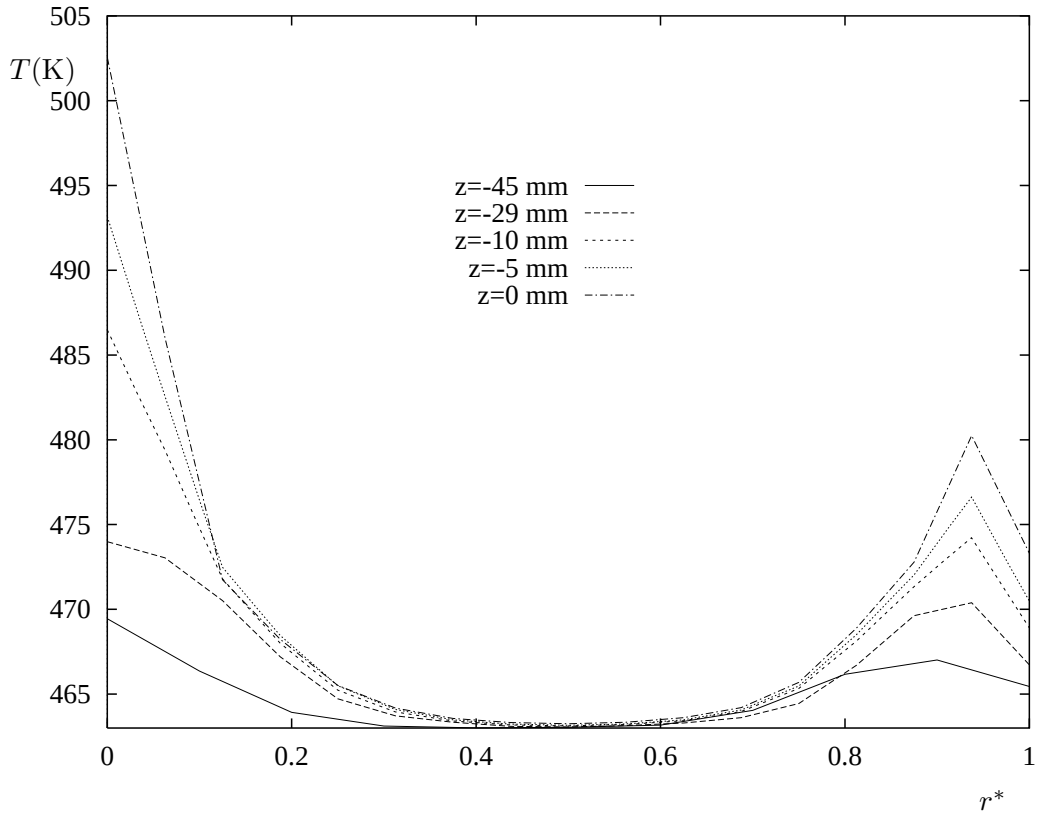

Wapperom, Fig. 3

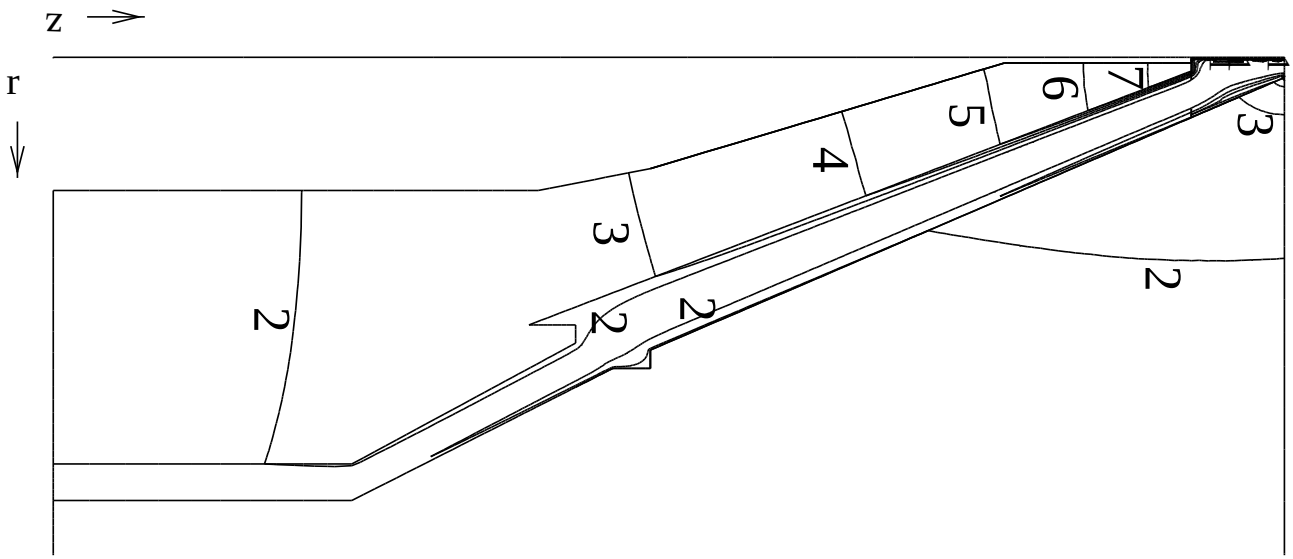

Wapperom, Fig. 4

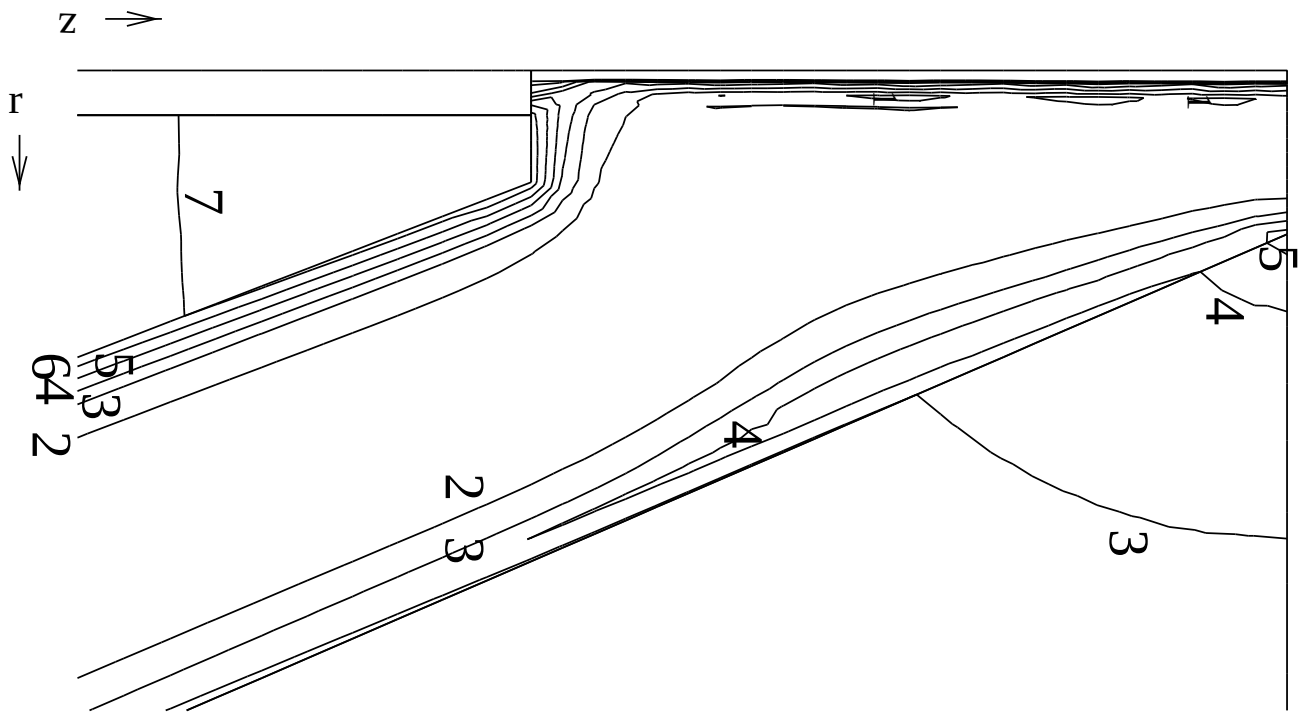

Wapperom, Fig. 5

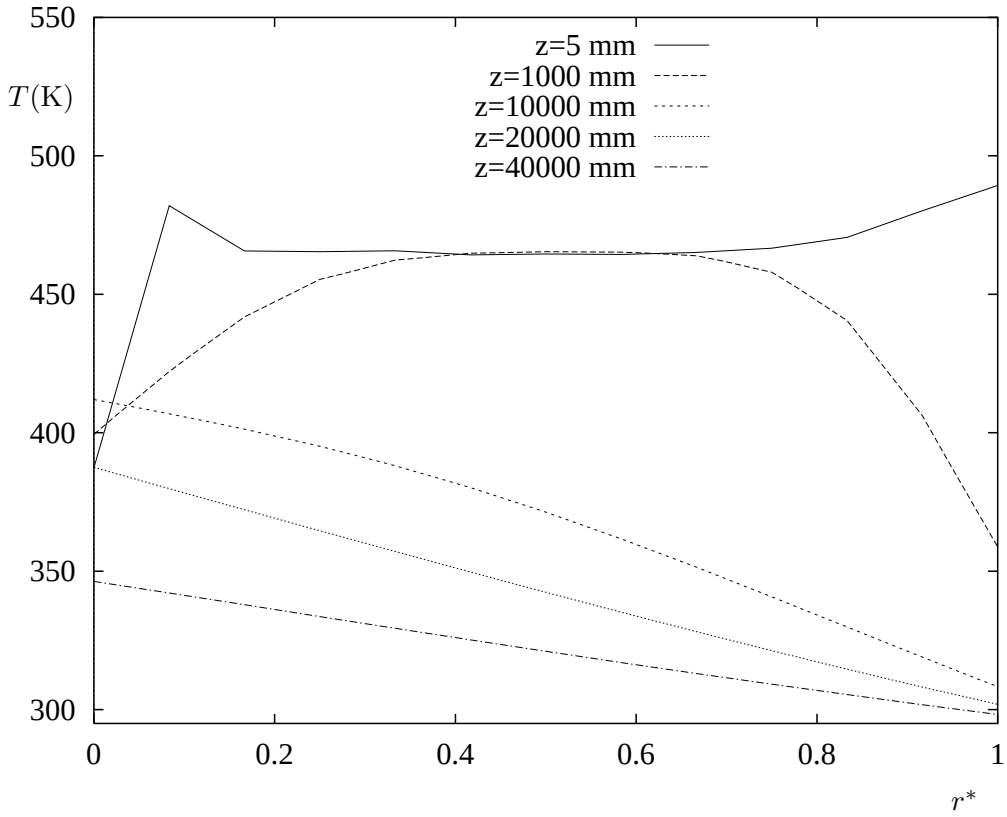

Wapperom, Fig. 6

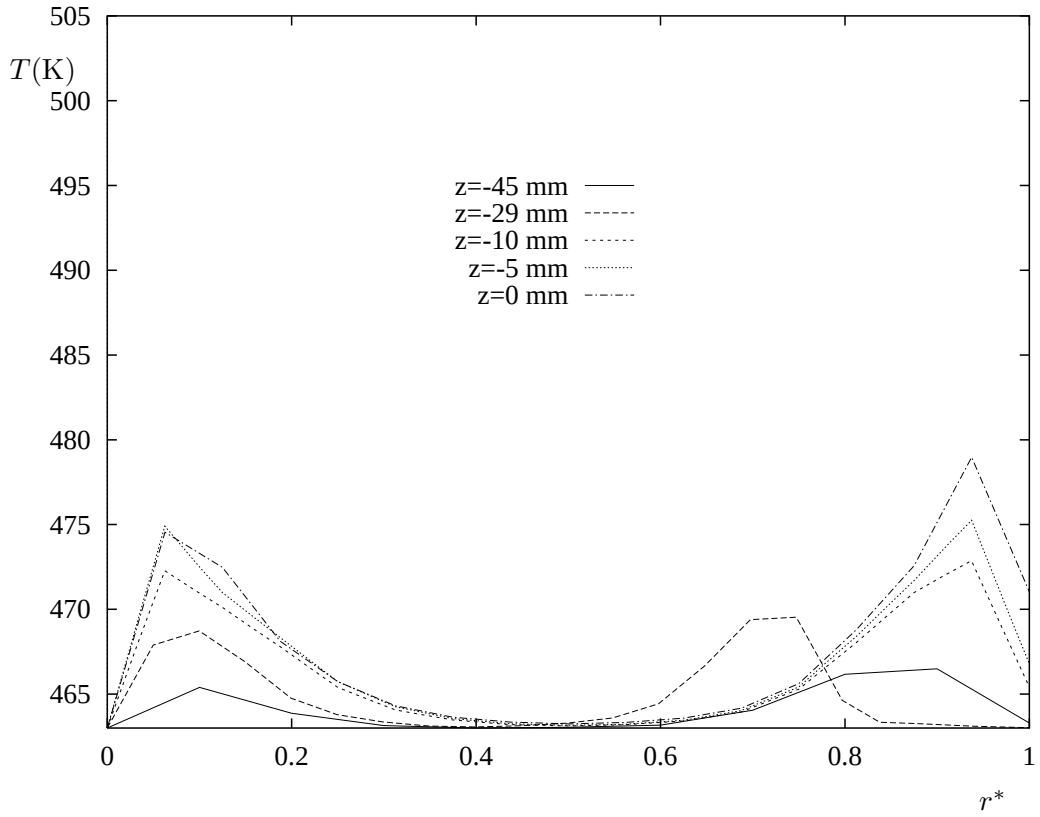

Wapperom, Fig. 7

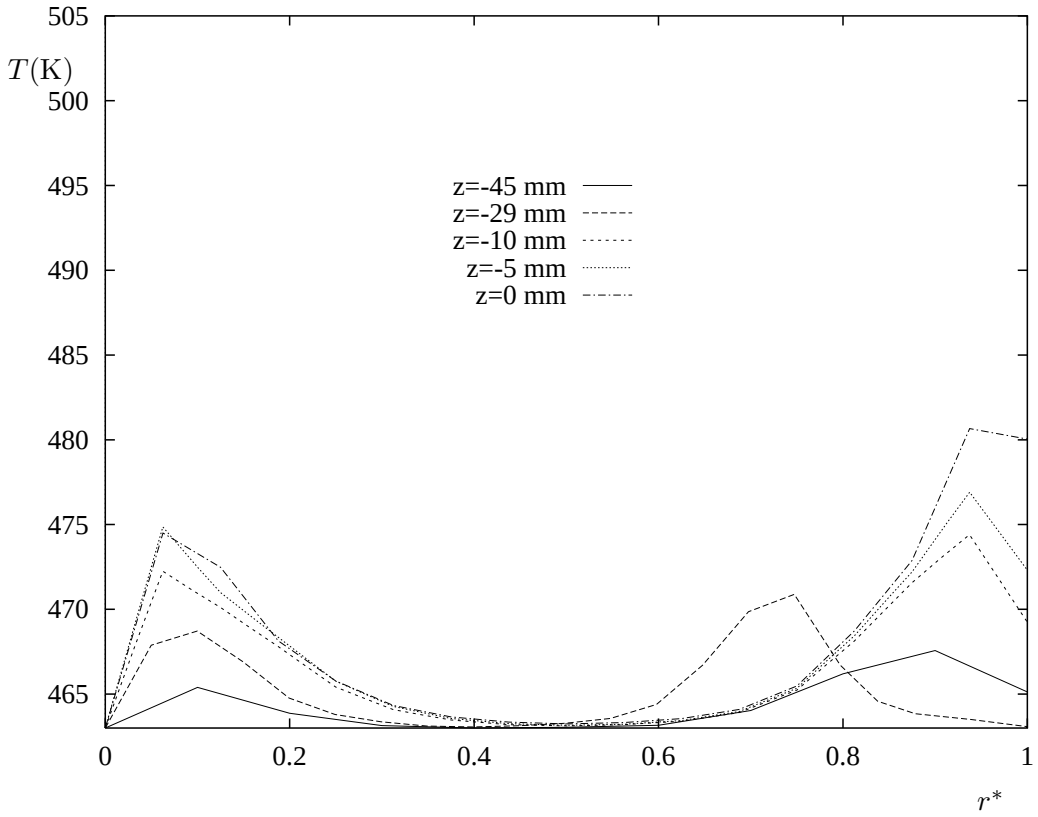

Wapperom, Fig. 8

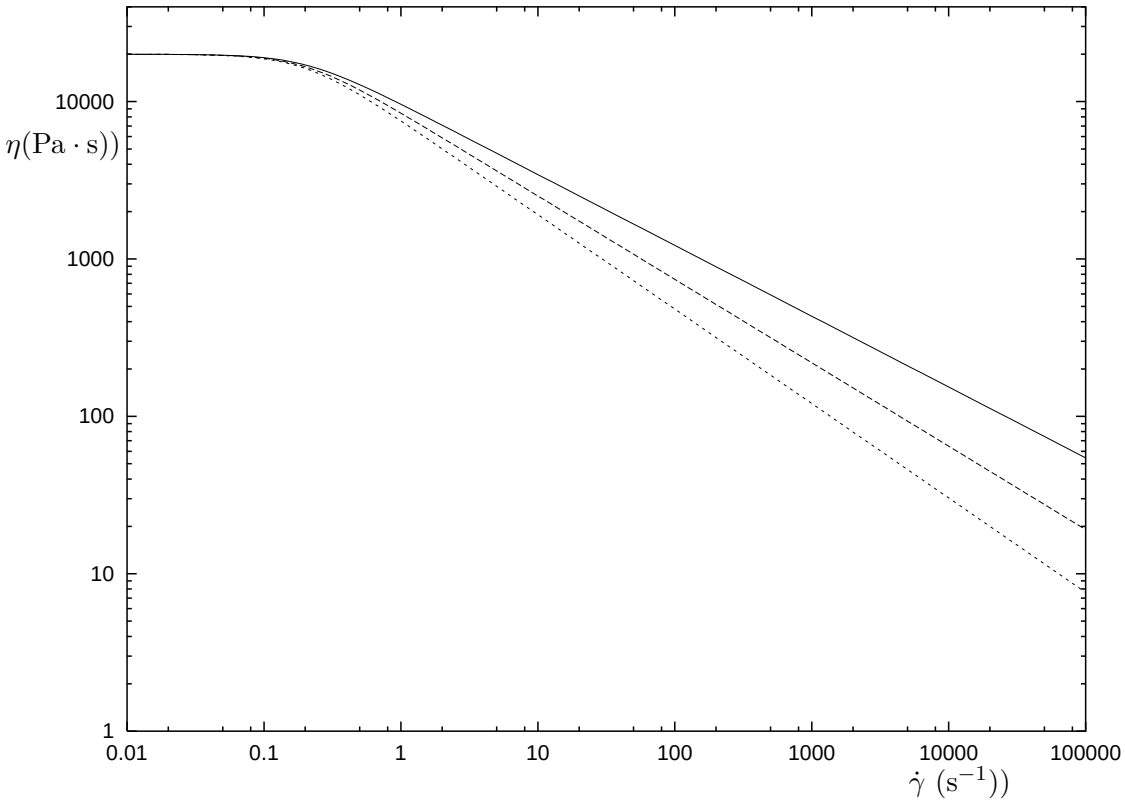

Wapperom, Fig. 9